Pore-level modeling of wetting

Martin J. Blunt

Department of Petroleum Engineering, Stanford University, Stanford, California 94305-2220

Harvey Scher

Department of Environmental Sciences and Energy Research, Weizmann Institute, 76100 Rehovot, Israel

(Received 8 June 1995)

The displacement of one fluid by another in a porous medium is influenced by the competition between advance through the centers of the pore space and flow of a wetting phase along crevices; different pore filling mechanisms whose threshold capillary pressures depend on the number of filled neighbors; and the perturbative effects of viscous and capillary forces. We present a three-dimensional pore-level model that represents these effects, including flow in crevices, and discuss the types of behavior that can result. Viscous and buoyancy forces introduce a finite correlation length for both the advancing front and for the trapped nonwetting phase. We use the percolation theory to derive expressions for the correlation length and the shift in trapped saturation for different flow regimes. When cooperative pore filling is significant, the average finger width is much larger than a single pore length, and percolation theory cannot predict the trapped saturation, even if asymptotically the fluid pattern is percolationlike. The type of fluid pattern changes with flow rate because of the competition between flow in crevices and frontal advance. This in turn can lead to a significant decrease in trapped nonwetting phase saturation with flow rate. This is a mechanism for a reduction in trapped saturation at much lower capillary numbers than that predicted using percolation theory or from considering mobilization of ganglia.

PACS number(s): 47.55.Mh, 64.60.Ak

I. INTRODUCTION

Soaking up liquid with a paper towel, the rising of the water table, and waterflooding an oil reservoir are all examples of wetting in porous media. Depending on the geometry of the porous medium, the contact angle, and the flow rate, a wide variety of different wetting patterns are possible (see, for instance, [1] for a thorough review). Capillary forces at the pore scale can allow ganglia of the displaced, nonwetting fluid to be trapped. In waterflooding an oil reservoir, typically 40% of the oil is trapped by water. In contrast, a wetting advance in relatively homogeneous media at high flow rates can leave little or no trapped nonwetting phase. In this paper we use a network model, based on an analysis of the pore scale physics of flow, to simulate a wetting invasion. The model can reproduce the wetting patterns seen experimentally, and is used to study the change in trapped nonwetting phase saturation with flow rate.

We represent a granular pore space (as seen in soil and rock) as an array of wide pores interconnected by narrower regions, which we call throats, as illustrated in Fig. 1. We further assume that the pore spaces have an angular or rough cross section, rather than being smooth cylinders. The wetting fluid preferentially resides in the corners or roughness in the pore space, which in this paper we will call crevices. A connected network of crevices acts as a conduit for the flow of wetting fluid, even if the centers of the pore space are occupied by nonwetting fluid. A treatment of this behavior is one of the main topics of this paper.

If the displacement is quasistatic, at the interface between the fluids, the pressure difference is given by the Young-Laplace equation

$$P_{cap} = P_{nw} - P_w = \gamma \left[\frac{1}{r_1} + \frac{1}{r_2} \right] , \qquad (1)$$

where nw and w label the nonwetting and wetting phases, respectively, γ is the interfacial tension, and r_1 and r_2 are the principal radii of curvature of the fluid interface. Displacement proceeds by making small changes in the capillary pressure, and allowing the fluids to reach different positions of equilibrium. If we consider the invasion of a wetting fluid, the capillary pressure starts at some high value and is progressively decreased. The wetting phase preferentially invades the smallest regions of the pore space first—crevices and throats, rather than larger pores.

There are two distinct types of advance. The first is pistonlike, where the fluid advances in a connected front occupying the centers of the pore space. In the second the wetting fluid flows along crevices in the pore space [the corners of the throat in the idealized illustration, Fig. 1(b)], filling pores in advance of the connected front.

First consider a pistonlike, or connected, advance. For a cylindrical throat of inscribed radius r, as illustrated in Fig. 1, the capillary pressure at which this occurs is

$$P_{cap} = \frac{2\gamma \cos\theta}{r} , \qquad (2)$$

(a)

(b)
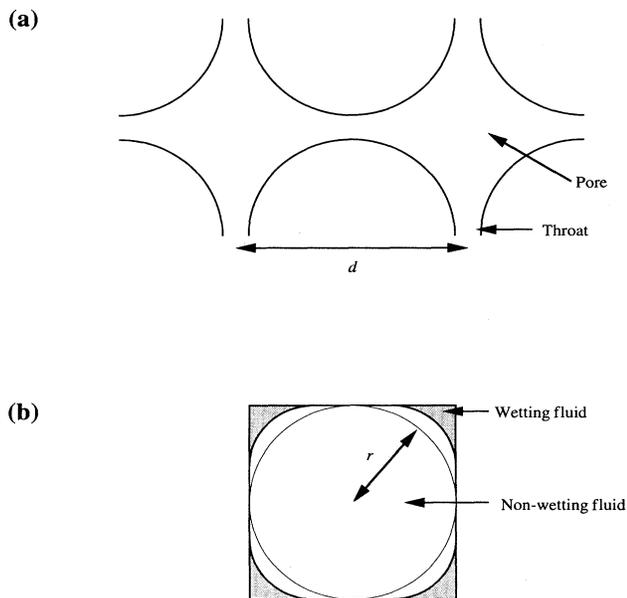
FIG. 1. Schematic of a porous medium. (a) The porous medium is considered to be an array of pores connected by narrow throats. (b) We assume that the pores and throats are angular in cross section, as shown, with an inscribed radius r.

where r is the inscribed radius of the throat and θ is the contact angle. The filling of pores is more complex, and depends on the number of nearest neighbors that are already filled with wetting fluid. Lenormand and co-workers [2,3] observed and described these processes. Figure 2 shows schematically how a pore may be filled when one or more of its surrounding throats are filled with wetting fluid. The process is limited by the largest radius of curvature necessary to fill the pore. This threshold curvature is dependent on the number of surrounding throats filled with wetting fluid. For a lattice of coordination number z, there are z such imbibition mechanisms, called I_0 to I_{z-1}, which represent filling of a pore when zero to $z-1$ connecting throats contain nonwetting fluid. The capillary pressures are ranked $P_{cap}(I_0) > P_{cap}(I_1) > \cdots > P_{cap}(I_{z-1})$. The I_0 mechanism can only occur if the nonwetting fluid is compressible. The I_z mechanism is impossible if the pores are larger than the throats, because in capillary equilibrium at least one of the attached throats must be occupied by wetting fluid before the pore is filled.

The second type of filling mechanism is called snap-off [4]. As the capillary pressure decreases, the radius of curvature of the fluid interface increases, and the layer of wetting fluid occupying the crevices of the pore space will swell. There comes a critical point where further filling of the crevices causes the interfacial curvature to decrease. At this point an instability develops, and the center of the pore space spontaneously fills with wetting fluid. For a throat with a square cross section, illustrated in Fig. 1(b), an instability occurs when the nonwetting

fluid is no longer in contact with the wall of the throat. This occurs at a capillary pressure [2]

$$P_{cap} = \frac{\gamma(\cos\theta - \sin\theta)}{r} . \tag{3}$$

Notice that this pressure is always lower than the corresponding pressure for a pistonlike advance, Eq. (2). Hence snap-off will only occur if the pistonlike displacement is topologically impossible, because there is no neighboring pore filled with invading fluid.

The competition between the pistonlike advance in throats, different types of pore filling, and snap-off lead to several different types of displacement patterns. The flow regime is controlled by the flow rate (which influences the extent of flow in crevices), the contact angle (which affects the competition between pore and throat filling [5,6]), and the geometry of the pore space. The different types of possible displacement pattern are as follows.

(1) Bond and site percolation. If the flow is very slow and the invading fluid is completely wetting, the invading fluid will occupy the crevices of the pore space throughout the system. As the capillary pressure drops, the throats will be filled in order of radius, with the narrowest filling first [2,7]. This corresponds exactly to bond percolation. If the pores are much larger than the throats, and the displaced fluid is compressible, after all the throats have filled the pores will fill, again in order of size, by the I_0 mechanism. This is site percolation and is shown in Fig. 3(a).

(2) Invasion percolation. This occurs when the invading fluid is nonwetting and hence does not occupy the crevices of the pore space. In this case the advancing fluid attempts to occupy the widest portions of the porous medium, and the capillary pressure rises as the displacement proceeds. At every stage in the process the largest throat adjacent to a filled pore is invaded. Any pores connected to filled throats are automatically filled, since they are larger than the throats. The fluid pattern then resembles the infinite cluster in a bond percolation process. This type of advance is called invasion percolation [8–10], and has been observed experimentally [11]. The invasion of a wetting fluid, without flow in crevices, when there is a very wide distribution of pore radii, will also be an invasion percolation process, if the pores are much larger than the throats. Here the advance is impeded by pore filling, and the fluid fills the smallest pore adjacent to an already filled throat. The fluid pattern, shown in Fig. 3(b), resembles the infinite cluster in a site percolation process.

(3) Flat frontal advance. If we consider a wetting invasion where there is no flow in crevices, the fluid advance is impeded by the pores. If the pore size distribution is quite narrow, and the pores are only slightly larger than the throats, the pores fill most readily when surrounded by other filled pores. This leads to the advance of a flat connected front, and has been observed in micromodels [2]. This is illustrated in Fig. 3(c), where the fluid advances as an I_3 mechanism followed by a cascade of more favorable I_2 processes that fill a layer of pores with wetting fluid.

(4) Nucleated faceted cluster growth. At low flow rates, where there is transport of wetting fluid in crevices, it is possible for the pores to fill by a cluster growth mechanism. This is analogous to case (3) above, and also occurs when the pores all have fairly similar sizes and are only slightly larger than the throats. The filling of a small number of throats by snap-off allows some pores to be invaded by one of the I_n mechanisms. This allows more throats to be filled, and can initiate further pore filling. In this case faceted clusters of filled pores begin to grow and one of them will eventually invade the whole network. This process has been described in detail [2,12], and is shown in Fig. 3(d).

(5) Self-affine growth. When there is competition between throat and pore filling mechanisms, which occurs at intermediate contact angles, or where there is a fairly wide distribution of pore and throat sizes, a distinct wetting pattern is observed intermediate between invasion

(a)

(b)

(c)

(d)

(e)

(f)
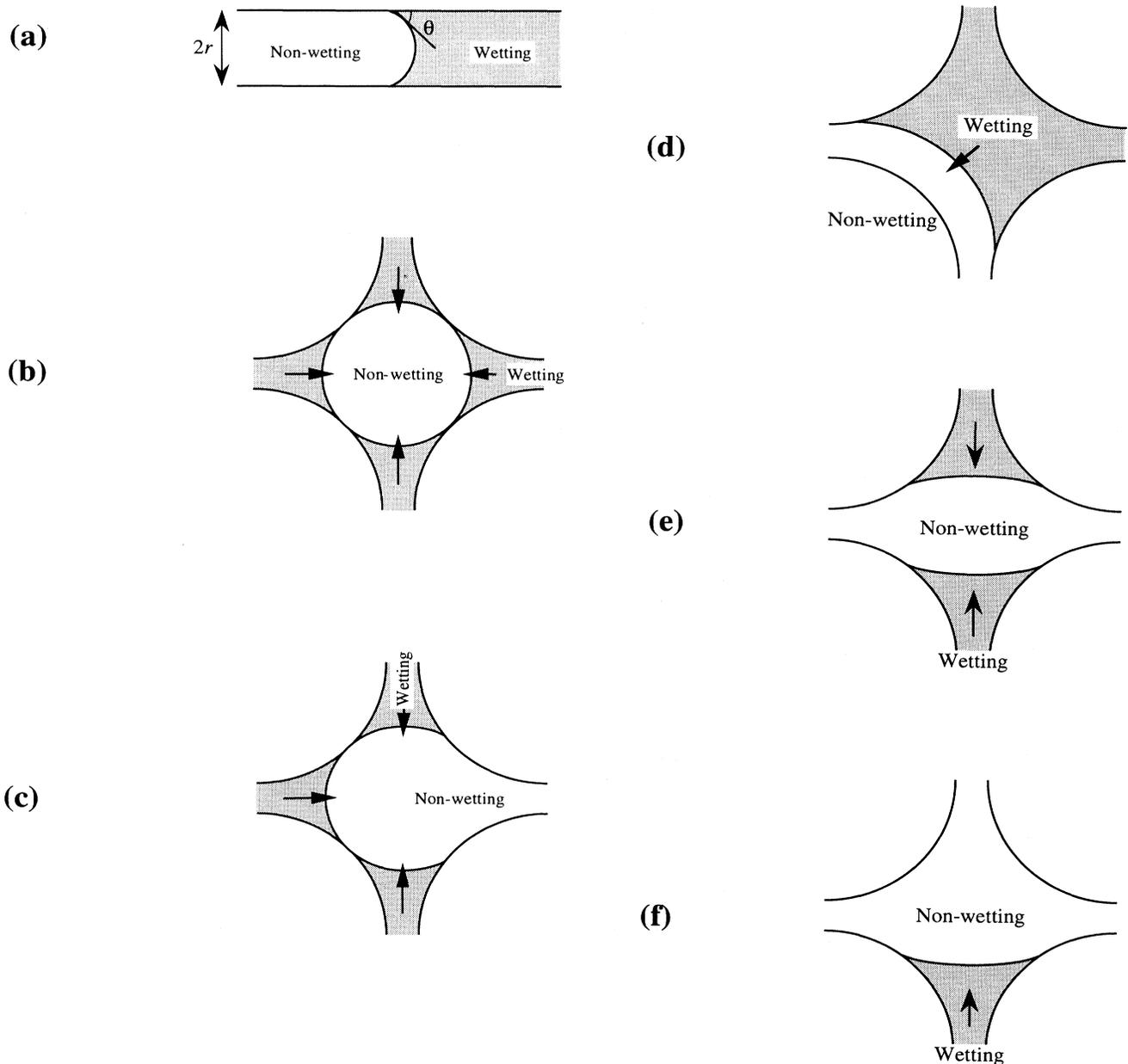
FIG. 2. Different types of pistonlike advance. (a) Throat filling at a capillary pressure $P_{cap} = 2\gamma \cos\theta / r$. (b) I_0. This mechanism only occurs when the nonwetting fluid is compressible. (c) I_1, when one neighboring throat is filled with nonwetting fluid. (d) I_2, when two of the adjacent throats are filled with nonwetting fluid. (e) I_2, when the two filled throats are opposite each other. In this paper we will assume that both types of I_2 event occur at the same capillary pressure. (f) I_3.

percolation [case (2)] and flat frontal advance [case (3)]. Macroscopically the wetting front is flat, with an infinite finger width, but the advancing interface is self-affine. Such behavior has received careful theoretical and numerical study [5,13], and has been observed experimentally [14–17].

(6) Nucleated self-affine cluster growth. In analogy to case (5) above, there should be a regime when crevice flow occurs, where clusters of filled pores are nucleated and grow, but with a rough, self-affine interface, rather than a faceted front. This regime has not been observed.

The different types of wetting pattern described here

(a)
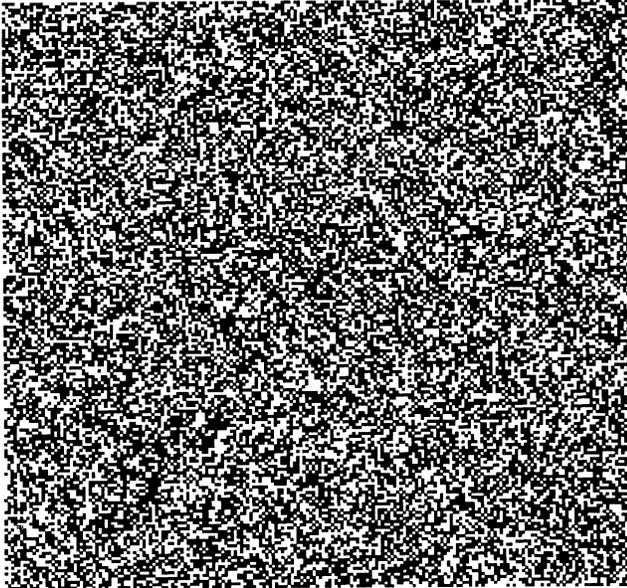
(b)
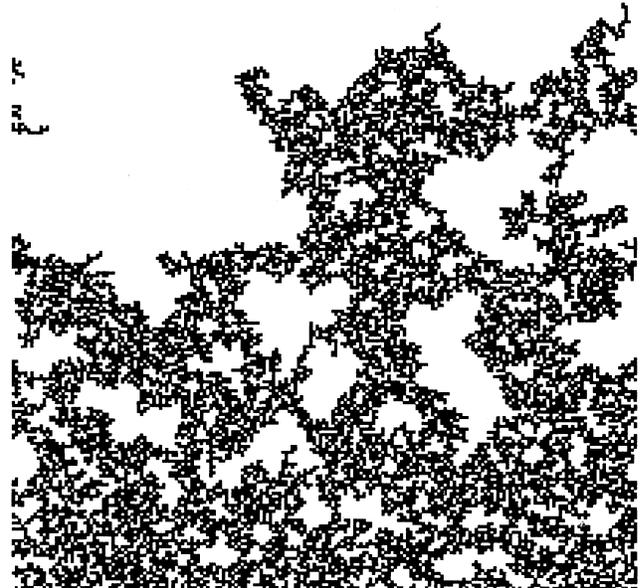
(c)

(d)
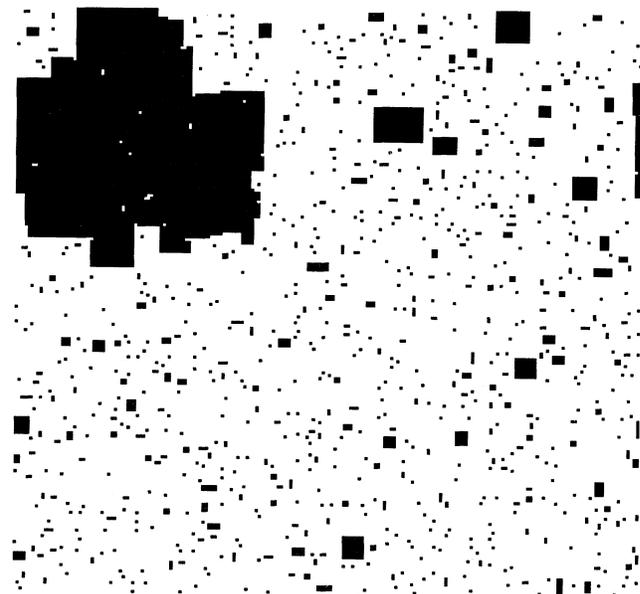
FIG. 3. Different types of wetting invasion, simulated using the network model described in the paper. The simulations are run on a 200×200 square network. Pores filled with wetting fluid are shown at breakthrough. The model parameters used for these simulations and those presented later are listed in Table I. (a) Site percolation. Pores are filled anywhere in the network in order of size. Flow in crevices provides fluid for filling a pore or throat anywhere in the system. (b) Site invasion percolation. This is similar to case (a), except that there is no crevice flow and hence we can only fill pores next to the connected front. (c) Flat frontal advance. Cooperative pore filling mechanisms allow the fluid to advance as a flat front. (d) Nucleated faceted cluster growth. This is similar to case (c), except that flow in crevices allows pores and throats to be filled anywhere. These act as nucleation sites for cluster growth. In this figure we are before breakthrough. The largest cluster will continue to grow and eventually will fill the system.

are equivalent to those observed for diffusion percolation [18], as described by Ji and Robbins [13]. In diffusion percolation, bonds are filled at random with some probability p. Then all bonds with more than n nearest neighbors are also filled. For n close to the coordination number of the lattice, the percolation transition is a normal, second order process. For larger n the percolating probability becomes infinitesimally small, and the percolating transition is first order with the growth of nucleated clusters. The full range of behavior for diffusion percolation has not been studied, and so it is not known if the six cases enumerated above are an exhaustive list of possible phenomena.

Recently self-affine wetting fronts have received considerable experimental and theoretical attention [5,13–17], as has the crossover from invasion percolation, to self-affine growth to flat frontal advance [5,6,13,19,20], which is characterized by a diverging finger width W [6,13]. This paper will not study these issues, but will discuss the effects of transport in crevices and the influence of viscous and buoyancy forces.

We will present a numerical model for fluid displacement, based on local capillary equilibrium that accounts for buoyancy and flow in crevices. The model, however, does not explicitly compute the viscous pressure gradient in the system. The combined effects of viscous and capillary forces have been studied in network models of drainage that include an explicit solution for the pressure field [21–23]. Computing the pressure when the crevice flow is significant limits the studies to fairly small two-dimensional systems [24]. We will use a simple model to account for the viscous pressure drop due to flow in crevices, which is similar in concept to the method used by Oren, Billiotte, and Pinczewski to study spreading films of oil in three phase flow [25]. We will show that, in many cases, viscous and gravity forces introduce quite a short correlation length into the system, meaning that the fluid pattern is not clearly in any of the regimes mentioned above. For this reason, we will not attempt to find the asymptotic flow regimes, when there are no viscous or gravity forces, for the cases we study.

We will study the effect of the flow rate on the saturation of the trapped nonwetting phase (the residual saturation). The capillary number, which we define below, is a dimensionless ratio of viscous to capillary forces. The decrease in residual saturation with increasing capillary number has received extensive experimental and theoretical study (see Chap. 5 of [26] for a review). The experiments that investigate this effect are of two types. The first performs an imbibition at some low flow rate until the entire nonwetting phase is trapped. Then the flow rate is increased, and the decrease in trapped saturation is measured. This studies the effects of flow rate on the discontinuous nonwetting phase. The second involves imbibitions at different flow rates, from which the residual saturation as a function of the capillary number is measured. Here the nonwetting phase is continuous until the end of the experiment. In the first type of experiment, trapped ganglia of nonwetting fluid are mobilized. However, it is the second type of experiment that is more useful for an understanding of wetting under different physi-

cal conditions. In this case, an explanation invoking the mobilization of ganglia is unsatisfactory for two reasons. First, the continuous nonwetting fluid shows an appreciable shift in residual saturation at capillary numbers one to two orders of magnitude smaller than for discontinuous fluid [27–29]. Moreover, Abrams observed in his experiments that once the nonwetting phase is trapped, a significant decrease in residual saturation cannot be achieved by a subsequent 100 to 500 fold increase in the flow rate [30]. These observations cannot be explained by any sort of mobilization argument. Second, the capillary number at which we first see a noticeable reduction in residual saturation is of order 10^{-6} in micromodels [27] and in consolidated rock [28–31]. An analysis of pore-level forces predicts that a ganglion the size of a single pore will be mobilized at capillary numbers around 10^{-3}, which is the capillary number for which the residual saturation drops to zero for both types of experiments. However, to explain the fact that the residual saturation begins to decrease at much lower flow rates, we have to assume that some very large ganglia, of order 1000 pore lengths across, are mobilized. However, these ganglia will break into smaller blobs and then, one assumes, they will not be recovered. Percolation theory has been used to predict the shift in trapped saturation with viscous and buoyancy forces [7,32,33] for continuous nonwetting fluid. During imbibition, viscous forces prevent the formation of large clusters. These large clusters are broken up into smaller ganglia, and it can be shown that the net effect is a decrease in residual saturation. However, as we will show below, these arguments still fail to predict a significant effect on residual saturation at capillary numbers around 10^{-6} and lower.

At a very low flow rate, flow in crevices allows snap-off throughout the system and a large fraction of the nonwetting phase can be trapped. In contrast, at higher flow rates, snap-off is suppressed and a connected fluid front advances which will trap less nonwetting fluid. As we will show below, since the flow resistance in crevices is large, we find that the suppression of snap-off causes a significant decrease in residual saturation at capillary numbers of around 10^{-8} and above. The observation that the change in residual saturation with capillary number is due to changing morphology of the wetting fluid advance is obvious from the experimental work in two-dimensional micromodels performed by Lenormand and Zarcone [2,27]—capillary numbers as low as 10^{-8} were needed to observe imbibition dominated by snap-off events, while capillary numbers larger than 10^{-4} gave a frontal advance with very little trapping. Zhou and Orr analyzed trapping on the pore scale under the influence of both viscous and buoyancy forces, and performed a series of experiments that measured the residual saturation for different capillary and Bond numbers [34]. Their results were consistent with a theoretical model that incorporated the effects of crevice flow on the displacement pattern.

In Sec. II we present a numerical network model that accounts for different pore filling mechanisms and flow in crevices. Then we define capillary and Bond numbers and express the model parameters in dimensionless form.

In Sec. IV we show example results in different flow regimes and define a finger width. In Sec. V we derive the correlation length due to viscous and buoyancy forces using percolation theory, when there is no crevice flow. We will show that the predictions of percolation theory are limited to displacements with a small finger width, where cooperative pore filling is not significant. In Sec. VI we discuss crevice flow and the transition from connected advance to a displacement dominated by snap-off as we decrease the capillary number. We also derive the viscous correlation length when there is significant crevice flow. In Sec. VII we discuss the change in residual saturation with flow rate.

II. NUMERICAL MODEL

The porous medium is modeled as a cubic or square array of pores connected by throats. The throat radii r are selected at random uniformly from λ to 1, where $0 \leq \lambda \leq 1$. Other distributions of radii would be possible. In order to be able to reproduce all types of fluid advances, we specified the threshold radii for filling by each of the I_n mechanisms separately. These in reality are controlled by the pore size, its shape, and the shape of the connecting throats, as well as the contact angle. The mean radius of curvature for filling by an I_n mechanism is computed as follows:

$$R_n = R_0 + \sum_{i=1}^{n} A_i x_i , \qquad (4)$$

where the x_i are random numbers chosen uniformly from 0 to 1, and the A_i are input parameters. R_0, the radius of curvature for the I_0 mechanism, is chosen such that it is consistent with the pores being larger than any of the surrounding throats:

$$R_0 = \max(r_i, A_0 x_0) , \qquad (5)$$

where r_i labels all the surrounding throats, x_0 is a random number between 0 and 1, and A_0 is an input parameter. The critical capillary pressure for pore filling, when the pore has n adjacent unfilled throats is

$$P_{\text{cap}} = \frac{2\gamma}{R_n} . \qquad (6)$$

The capillary pressure for pistonlike filling of a throat, which is connected to a filled pore, is $2\gamma/r$, while the capillary pressure for snap-off is γ/r. From a comparison of Eqs. (2) and (3), this represents a flow with a contact angle of zero. However, in a dimensionless form of the equations (outlined in Sec. III), we can represent flow at any contact angle implicitly through the relative values of the different pore filling parameters.

We assume that the pressure drop across regions of the network completely saturated with invading fluid is negligible, but that the pressure drop along narrow wetting layers in the crevices of the pore space is significant. Consider that a pore or throat is filled, and that the fluid is provided by flow along a crevice of length l, as shown schematically in Fig. 4. The flow rate is Q. The relationship between the pressure gradient and flow rate is
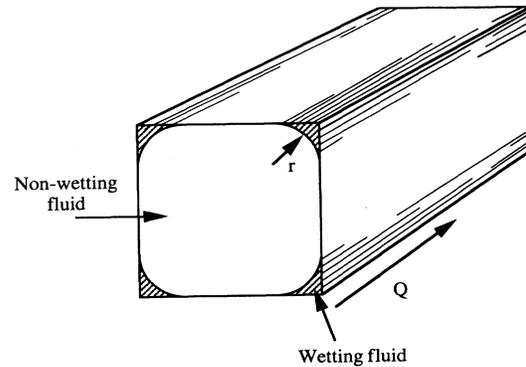
FIG. 4. Crevice transport. Fluid to fill pores and throats is supplied ahead of the connected front by flow in the corners of the pore space.

$$Q = -\frac{r^4}{\beta\mu} \frac{dP}{dx} , \qquad (7)$$

where μ is the fluid viscosity and r is the local radius of curvature in the corner. P is the pressure in the advancing (wetting) phase. We assume that the pressure in the nonwetting phase is zero. β is a dimensionless conductance factor. Equation (6) is a generalized form of Poiseuille's law for flow in corners. β depends on the geometry of the pore and the boundary condition at the phase boundary. For instance, for a square crevice and a fluid with a contact angle of zero, finite element calculations have shown that $\beta = 109$ if there is no slip at the nonwetting/wetting fluid interface and 290 if there is no flow at the interface, while for a triangular crevice β varies from 15 to 32 depending on the boundary condition at the fluid interface [35]. We assume that locally the interface is in capillary equilibrium and hence $P = -P_{\text{cap}} = -\gamma/r$; then

$$Q = -\frac{\gamma^4}{\mu\beta P^4} \frac{dP}{dx} . \qquad (8)$$

This expression can be integrated to find

$$P_0 = \frac{P_{\text{cap}}}{\left[1 + \dfrac{3\beta P_{\text{cap}}^3 Q\mu l}{\gamma^4} \right]^{1/3}} , \qquad (9)$$

where P_0 is the capillary pressure at the beginning of the crevice, equivalent to the inlet pressure in our model, and P_{cap} is the local capillary pressure where the element is being filled—either pistonlike throat filling, throat filling by snap-off, or pore filling.

We consider fluid injection from one face of a rectilinear system. Fluid leaves through the opposite face and there are periodic boundary conditions on the other faces. If the injected fluid is wetting, it will have a lower pressure than the fluid it displaces. The wetting phase pressure at the inlet is progressively increased, corresponding to a decrease in capillary pressure. The capil-

lary pressure at the inlet P_0 necessary to fill an element anywhere in the network is calculated using Eq. (9). P_{cap} is found using the expressions quoted previously for pore and throat filling. l is the minimum distance from the element to the inlet, where the path length through completely filled tubes or throats is zero. These pressures are stored in a sorted list. The element that has the highest capillary pressure is the next to be filled. Once the element is filled, l is recomputed for the whole network. If the number of filled throats adjacent to any of the pores has increased, the pore filling capillary pressures are updated to represent different I_n mechanisms.

The model represents the competition between the advance of the connected phase and flow in corners, but makes several approximations. We ignore any pressure drops in the displaced phase and in the portions of the network completely saturated by the wetting fluid. We will show that, below a viscous correlation length, this is a good approximation, but on the large scale, particularly when the fluid pattern is percolationlike, the effects of pressure drops in the centers of pores and throats are significant. We also use a simple method to compute the pressure drop for flow in corners. This is a reasonable assumption in regions of low wetting phase saturation, where the nonwetting phase is well connected and the flow rates in each crevice are approximately constant.

The model allows for both compressible and incompressible displaced fluid. Displacement proceeds as described above for compressible flow. If the displaced fluid is incompressible, an element is only filled if there is a connected pathway to the outlet of pores and throats filled with displaced fluid.

We can model cases where crevice flow is not allowed, by only allowing pores adjacent to already filled pores to be filled. In this case we do not need to account for throats explicitly, since all the throats adjacent to a filled pore will be also filled, and no throats may be filled unless they are adjacent to a filled pore. This simplifies the model considerably.

Density differences between fluids are also included. We assume that the principal flow direction is vertical. Then we add an extra term to Eq. (9) to accommodate buoyancy forces:

$$P_0 = \frac{P_{cap}}{\left[1 + \dfrac{3\beta P_{cap}^3 Q \mu l}{\gamma^4}\right]^{1/3}} - (\rho_w - \rho_{nw})gh , \qquad (10)$$

where ρ is the fluid density, g is the acceleration due to gravity, and h is the height.

III. CAPILLARY AND BOND NUMBERS

The competition between pore and throat filling and flow in crevices and bulk advance, together with the perturbative effects of viscous and gravity forces, lead to several different length scales. Possibly the most subtle effect is that of viscous forces on the flow.

Conventionally a capillary number that measures the ratio of viscous to capillary forces in the system is defined

as follows:[26]

$$N_{cap} = \frac{\mu q}{\gamma} , \qquad (11)$$

where q is the volume of fluid injected per unit time per unit area. The ratio of buoyancy and capillary forces is measured by a Bond number, defined by

$$B = \frac{(\rho_w - \rho_{nw})gr^2}{\gamma} , \qquad (12)$$

where r is a representative pore size.

The multiphase Darcy law for the flow of wetting and nonwetting phases may be written

$$q_w = -\frac{Kk_{rw}}{\mu_w}\nabla(P_w + \rho_w gh) , \qquad (13)$$

$$q_{nw} = -\frac{Kk_{rnw}}{\mu_{nw}}\nabla(P_{nw} + \rho_{nw} gh) . \qquad (14)$$

Then the ratio of a typical viscous pressure drop between two pores separated by a distance d to a capillary pressure, when the relative permeability k_r is of order 1 is $\mu q dr / \gamma K$. The permeability K and a typical pore size are related by $K = \delta r^2$, where δ is a small parameter representing the connectivity of the medium. If we considered the porous medium to be a regular cubic array of cylindrical tubes, radius r and spacing d, then, using Poiseuille's law, we would find $\delta = \pi r^2 / 8d^2$. We define $a = d/r$, the ratio of a pore-throat length to a typical radius, which will be in the range 5–10. Hence δ is approximately 4×10^{-3}–1.6×10^{-2}. Real porous media have tortuous flow pathways, and we would expect δ to be lower than this. For instance, for a random close packing of spheres of radius R, $K \approx 2.7 \times 10^{-3} R^2$ [36,37]. A typical pore radius is likely to be smaller than a grain radius, but in more consolidated media, with poorly connected flow pathways, the permeability may be very low, even if some of the channels are quite large. For most porous media we expect δ to be of order 10^{-3}. a/δ is a dimensionless measure of the flow resistance in a single pore. The ratio of viscous to capillary pressures at the pore scale is $(a/\delta)N_{cap}$ or up to 1000–10 000 times larger than N_{cap}. Hence when viscous and capillary pressure drops are of the same magnitude in a single pore, the conventional capillary number will be around 10^{-3} or even smaller. For instance, this implies that oil ganglia a few pore spaces across will be mobilized by viscous forces at capillary numbers of around 10^{-3}–10^{-4}, which is roughly in accord with experimental data [28]. Typical flow rates in oil reservoirs range from around 1 m/day to 1 m/year, except near wells. Natural acquifer flows are about as slow, but during pumping flow rates up to 100 m/day can be achieved. If we consider the flow of water and air ($\mu = 10^{-3}$ kg m^{-1} s^{-1}, $\gamma = 70$ mN m^{-1}) this gives capillary numbers in the range 10^{-5}–10^{-10}. Even lower capillary numbers may be typical for the slow flow of viscous oils, while for nearly miscible gas injection into oil reservoirs, with interfacial tensions of 0.1 mN m^{-1} and lower, capillary numbers of order 10^{-3} and above are possible.

The ratio of the buoyancy pressure to the capillary pressure over a single pore throat of length d is $(\rho_w - \rho_{nw})gdr/\gamma$ or aB. If we consider oil and water with a density difference of 100 kg m^{-3}, an interfacial tension of 40 mN m^{-1}, $a = 10$ and a typical throat radius of 20 μm, we find aB approximately equal to 10^{-4}. For air and water the density difference is ten times larger, and aB is of order 10^{-3}.

We can rewrite Eq. (10) in dimensionless form in terms of the capillary and Bond numbers. To do this we make an important approximation. We assume that, on average, the flow is uniform throughout the network, and that the flow in a crevice that is supplying fluid for pore or throat filling $Q = qd^2$. Then

$$P_0^d = \frac{P_{cap}^d}{[1 + 3\alpha N_{cap}(P_{cap}^d)^3 x_l]^{1/3}} - aBk \ , \tag{15}$$

where α is a crevice resistance factor,

$$\alpha = \frac{\beta d^3}{r^3} = \beta a^3 \ , \tag{16}$$

and the dimensionless pressures P^d are measured in units of γ/r, where r is a typical throat radius (unity by definition in our simulations), and x_l and k are dimensionless distances measured in units of the interpore length d. k is the height of the element. x_l is the minimum length of crevice necessary to reach the inlet, where the distance through completely filled elements is ignored. By assuming that $Q = qd^2$ for each crevice, we are able to identify a capillary number for our simulations.

IV. FLOW REGIMES AND FINGER WIDTH

Figure 3 shows example two-dimensional results from the numerical model for different input parameters, illustrating some of the flow regimes discussed above. Table I lists the model parameters for these and the other figures. The simulations presented in this paper are intended to cover the range of behavior seen experimentally, although we will not attempt to represent any single experiment or porous medium exactly.

We measure the finger width at breakthrough, when the wetting fluid first spans the system. Let us label a grid block by coordinates i, j, and k in the x, y, and z directions, respectively. The principal flow direction is in the vertical z direction. The simulation contains N_x by N_y by N_z grid blocks in total. We take a horizontal slice through the system at some fixed value of j and k. Then moving in the x direction, we count the number of times there is a filled pore next to an unfilled pore. However, for incompressible flow, we ignore unfilled pores that are trapped by wetting fluid. We repeat this for all possible values of j and k. W is defined as the total number of filled and trapped pores divided by the total number of filled/unfilled transitions. Cooperative pore filling may lead to very large values of the average finger width, even if, on even larger scales, the system is percolationlike.

In a two-dimensional square network, if all the I_3 events are less favorable than any I_2 event, we will see a flat frontal advance [6] or a faceted cluster growth [12]. This is because when I_3 occurs it will inevitably launch a cascade of cooperative filling events until the wetting front is smooth. By construction, the numerical model

TABLE I. Parameters used in the simulations presented.

Figure	grid size	Compressible[a]	Crevice flow[a]	$A_0 - A_5$[b]	λ	aB	αN_{cap}
3(a)	200×200	Y	Y	1 0 0 0	0	0	0
3(b)	200×200	Y	N	1000	0	0	0
3(c)	200×200	Y	N	1 0 0 100	0	0	0
3(c)	200×200	Y	Y	0 0 0 200	0.99	0	0
5(a)	512×512	Y	N	0 0 8 10	0	0	0
5(b)	512×512	N	N	0 0 8 10	0	0	0
6	64×64×128	N	N	2 0 0 0 0 0	0	0	0
6	64×64×128	N	N	2 0 0 0 1.4 1.4	0	0	0
6	64×64×128	N	N	2 0 0 0 2.4 2.4	0	0	0
7	32×32×64	N	N	2 0 0 0 c c for c	0	0	0
	for $W < 10$ and 64×64×128 for $W > 10$			between 0 and 2			
	with at least two runs for each value of c.						
8	512×512	N	N	0 0 8 10	0	0.001	0
9(a)	128×128	Y	Y	0 0 2 16	0	0	1.7
9(b)	128×128	Y	Y	0 0 2 16	0	0	$1.7×10^{-1}$
9(c)	128×128	Y	Y	0 0 2 16	0	0	$1.7×10^{-2}$
9(d)	128×128	Y	Y	0 0 2 16	0	0	$1.7×10^{-3}$
9(e)	128×128	Y	Y	0 0 2 16	0	0	$1.7×10^{-4}$
10,11,	32×32×32	N	Y	2 0 0 0 3 3	0	0	1.7–
12,13				2 00 0 1.4 1.4			$1.7×10^{-4}$
				0 0 0 2 4 6			

[a]Yes (Y) or no (N).

[b]For two-dimensional simulations only $A_0 - A_3$ are defined.

always allows for some overlap between I_3 and I_2, and this is evident in Figs. 3(c) and 3(d), where the fluid front is not completely flat, but shows some roughness. Some sites become pinned, and in an infinitely large system this will force the pattern to look percolationlike beyond some finger width W [13]. Hence, strictly speaking, Fig. 3(c) is asymptotically invasion percolation, while Fig. 3(d) is site percolation, but with a finger width clearly larger than the system size (200 in this case). In three dimensions it is possible for pinning to generate a self-affine surface, where the interface is rough, but the finger width is infinite [13]. While highly regular experimental porous media and numerical models may be found that allow completely faceted growth, it is unlikely that there is absolutely no overlap between I_3 and I_2 events in any real system. This will then lead to some form of rough interfacial advance with a large (or infinite) finger width. However, in order to see a truly asymptotic system, the experiment or numerical model will have to be quite huge, and on such a scale that viscous and buoyancy forces will have a significant influence. Thus the asymptotic regime may never be observed. In this paper we will not study the asymptotic behavior, but will investigate flow with capillary and Bond numbers representative of natural systems.

V. CORRELATION LENGTHS IGNORING FLOW IN CREVICES

In this section we will use percolation theory to analyze displacements where there is no flow in crevices. We show that some predictions of percolation theory are not valid when there is significant cooperative pore filling. Moreover, all discussion on correlation lengths in this paper is limited to percolationlike displacements, and does not apply to flat frontal advance or locally self-affine growth. Flat fronts have no structure anyway, but viscous and buoyancy forces will limit the size of the roughness seen in a self-affine growth. This issue will not be discussed here.

It is valid to ignore crevice flow in three circumstances: (i) the flow rate is sufficiently high that snap-off is completely suppressed, which occurs for capillary numbers of approximately 10^{-4} or higher; (ii) the invading fluid is not completely wetting, such that it does not naturally reside in angular corners of the pore space; and (iii) the pore space does not have a connected pathway of crevices, such as in smooth bead and sand packs. VI we will discuss flow in crevices.

In a percolationlike displacement we can define a percolation probability p when a fraction p of throats or pores are filled. The threshold value p_c is when a connected pathway of completely filled elements first spans an infinite system. Corresponding to this is a critical capillary pressure. Viscous and buoyancy forces impose a pressure gradient across the system, and hence the value of p varies with position. This means that infinite clusters at threshold are no longer seen, and there is a finite correlation length: below this length the system looks percolationlike, and above it the effects of viscous and buoyancy forces are apparent. We will now derive the correlation length for the different cases of interest, make predictions based on percolation theory, and compare the results with our simulations.

A. Trapping nonwetting fluid

If percolation theory is valid, the point at which the nonwetting fluid becomes disconnected (the terminal point) corresponds to its percolation threshold. The number of trapped clusters occupying s pores, $N(s) \sim s^{-\tau}$, where the exponent τ is approximately 2.18 in three dimensions [38]. A displacement with a finite finger width will be percolationlike beyond a distance W and will resemble[9] flat frontal advance on smaller scales. Thus only large clusters of size $s \geq W^D$ (where D is the fractal dimension of the clusters—2.53 in three dimensions) will be seen.

To test the percolation argument, we present simulation results for displacements without crevice flow with different finger widths. Figure 5 shows a 512×512 two-dimensional displacement at breakthrough, where the finger width is approximately 300. Figure 5(a) shows the displacement of a compressible fluid, where most of the surrounded fluid is contained in a single large cluster with relatively little volume contributed by smaller enclosed regions—we would predict that only large regions of order the finger width in extent would be trapped. In contrast, if the nonwetting fluid is incompressible, as shown in Fig. 5(b), many trapped regions of all sizes are present and the simple percolation theory argument is clearly not valid. Figure 6 shows the cumulative size distribution

$$M(s) = \sum_{s}^{\infty} sN(s) \sim s^{-\tau+2} \tag{17}$$

plotted for three three-dimensional displacements on a $64 \times 64 \times 128$ grid: one is an invasion percolation with trapping ($W=1.6$), the other has a finger width of 5.7, while the third allows some cooperative pore filling and the finger width is 17. The two cases with the smaller finger widths give distributions that are consistent with percolation theory, as shown previously [7]. However, we see no clear cutoff in the distribution at some size $s < W^D$. The example with the largest finger width does not look percolationlike at all. There is significant trapping of nonwetting phase clusters of all sizes, although the total number of trapped pores, $M(1)$, does decrease with finger width.

The fraction of trapped pores is $M(1)$ [Eq. (17)] divided by the total number of pores in the system. In this paper we will call the fraction of trapped pores the residual saturation. For a finger width of size W, percolation theory would predict $M(s) \sim W^{-D(\tau-2)} \sim W^{-\beta/\nu}$, for $s \leq W^D$, where we have used the scaling relation $D(\tau-2)=\beta/\nu$. The residual saturation is plotted as a function of finger width in Fig. 7 for a variety of three-dimensional displacements. Again, the agreement with percolation theory is poor—the best-fit exponent to the data was -0.59 ± 0.2, compared with the prediction $-\beta/\nu=-0.47$. Moreover, the data do not clearly follow

a power law.

The trapping of nonwetting fluid for displacements with different finger widths is not predicted by percolation theory. The reason for this is that at length scales below W the fluid front is not completely flat, and this allows some local trapping of small clusters. These small clusters make the dominant contribution to the residual saturation. The exact nature of this local trapping depends subtly on the capillary pressures for the different

FIG. 6. The cumulative trapped cluster distribution plotted as a function of cluster size on doubly logarithmic axes, for different finger widths W, as indicated. Percolation theory predicts that the graph should be a straight line of slope $2-\tau$, which is approximately -0.2. The distributions for the two plots with smaller finger widths are consistent with percolation theory, whereas the third case is not.

pore filling mechanisms, and is not easily represented in terms of just a single parameter.

B. Correlation length

We will now derive the correlation length due to the perturbative effects of viscous and buoyancy forces. This has already been discussed for systems where $W \approx 1$ [7,32,33]. We consider that the nonwetting fluid is about to become entirely trapped, and that its flow rate is negligible. In this case Darcy's law for the flow of wetting fluid can be written

(a)

(b)

FIG. 5. Connected fluid advance simulated on a 512×512 network. (a) Compressible flow with an average finger width of approximately 300. Notice that the majority of the surrounded nonwetting fluid is in one large cluster. (b) Incompressible flow. There is significant trapping of clusters much smaller than the finger width. This cannot be predicted by percolation theory.

FIG. 7. The trapped saturation as a function of finger width on doubly logarithmic axes. The best fit straight line has a slope of -0.59, compared with a percolation theory prediction of -0.47. Moreover, since the distribution of trapped clusters is not percolationlike, we have no reason to expect percolation theory to predict the change in trapped saturation.

$$q = \frac{Kk_r}{\mu} \nabla [P_{cap} - (\rho_w - \rho_{nw})gh] . \tag{18}$$

If the wetting phase is well connected, the relative permeability k_r is almost 1. This will be true if the residual saturation is small, but the relative permeability can be low, of order 0.1, if the nonwetting phase blocks the larger flow pathways [29]. Here we will assume that k_r is approximately 1. If the capillary pressure has some representative value $P_{cap} = \gamma / r$, and assuming that the direction of flow is vertical, then

$$\frac{r \nabla P_{cap}}{P_{cap}} \approx \frac{\mu q r^2}{\gamma K} + \frac{(\rho_w - \rho_{nw})gr^2}{\gamma} = N_{cap}/\delta + B . \tag{19}$$

The fractional change in capillary pressure is equivalent to a shift in percolating probability—p decreases in the direction of flow. This in turn limits the maximum size of a trapped cluster (the correlation length). ξ is defined as the correlation length measured in units of d. The average finger width is W. At the terminal point, when the defender is trapped, we call the shift in p across a correlation length ξ, $p - p_c$. From percolation theory $\xi/W \sim (p - p_c)^{-\nu}$, or $(p - p_c) = (\xi/W)^{-1/\nu}$, where the exponent ν is approximately 0.88 in three dimensions and $\frac{4}{3}$ in two dimensions [38]. From Eq. (19) the shift in p over a length ξd is approximately $a\xi(N_{cap}/\delta + B)$. Equating these two expressions gives

$$\frac{\xi}{W} \sim [Wa(N_{cap}/\delta + B)]^{-\nu/(1+\nu)} . \tag{20}$$

This is similar to the expression derived in [32,33], except here we have included the effects of both buoyancy and viscous forces together and included the effect of a finite finger width. Notice that the correlation length is controlled by the addition of both capillary and Bond numbers, as shown by Zhou and Orr [34]. This length will be much smaller than the macroscopic distance over which buoyancy forces and viscous forces combined are as large as the capillary force (of order $1/[a(N_{cap}/\delta + B)]$). When ξ/W is of order 1, the fluid pattern does not resemble a percolation cluster at threshold on any length scale. For large finger widths, this may occur even for representative values of the capillary and Bond number. We expect Eq. (20) to be correct, even if the distribution of trapped clusters is not percolation-like.

C. Shift in trapped saturation

A finite correlation length truncates the distribution of trapped clusters and leads to a decrease in residual saturation. It is possible to relate the fractional shift in trapped saturation to the correlation length by [7,32,33]

$$\frac{S(\xi = \infty) - S(\xi)}{S(\xi = \infty)} = \frac{\Delta S}{S} \sim \left[\frac{\xi}{W} \right]^{-(\beta + 1)/\nu} , \tag{21}$$

and thus

$$\frac{\Delta S}{S} \sim [Wa(N_{cap}/\delta + B)]^{-(\beta + 1)/(\nu + 1)} . \tag{22}$$

The analysis assumes that the distribution of trapped clusters can be described by percolation theory. Thus we only expect this expression to be valid for finger widths close to 1, or where there is no small-scale trapping of clusters on scales smaller than W. It has already been demonstrated that Eq. (22) can predict the change in residual saturation with buoyancy for trapping in imbibition, where the finger width is close to 1 [7].

Consider Fig. 8, which shows a two-dimensional, incompressible displacement, similar to Fig. 5, but where $Ba = 0.001$. Since the finger width is approximately 300, Eq. (20) predicts $\xi \sim W$. This is consistent with the picture where buoyancy has prevented large clusters from being trapped. However, we cannot use Eq. (22) to predict the change in residual saturation, since the small clusters still remain.

The conclusion of this section is that percolation theory does not predict the trapping of nonwetting fluid for systems with a large finger width. This is because on length scales below W, the fluid interface is not completely flat, and there is some trapping of small clusters. The exact amount of trapping is dependent on the details of the pore-level displacement. Even though we expect Eq. (20) for the correlation length to be valid, we cannot use it to predict the shift in trapped saturation, because the cluster size distribution does not follow percolation theory for large W.

D. Advancing wetting fluid

The next case to be considered is where there is no flow in crevices, and we derive the correlation length for the wetting phase at breakthrough. Below the correlation length, the pattern resembles invasion percolation with a
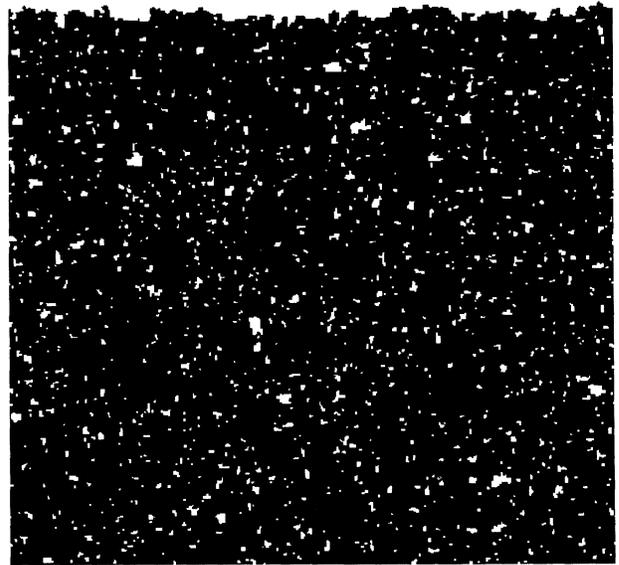
FIG. 8. Incompressible flow as in Fig. 5(b), but where $aB = 0.001$. The trapping of large clusters has been suppressed, but the smaller clusters remain.

finger width W, and, above it, the pattern will be statistically homogeneous with smooth changes in average saturation.

We develop the same argument as above. Again the shift in capillary pressure is dominated by the pressure gradient in the wetting phase. However, near breakthrough, the relative permeability is very small—if the shift in percolation probability is $p - p_c$, the relative permeability scales as $(p - p_c)^t$, where t, the conductance exponent, is approximately equal to 2.0 in three dimensions [38]. Moreover, the local flux of the wetting phase is lower than the injected flux, from which the capillary number is conventionally defined. Imagine that the speed of the front is v, and the flux is q_w, then, if the saturation is S, $v \sim q_w / S$. Just behind the front, where the wetting phase saturation is of order 1, the flow speed is approximately the same. Hence the flux at the advancing interface q_w is related to the injected flux q by $q_w \approx qS$. Again using percolation theory, the saturation is $S \sim (p - p_c)^\beta$, where β is 0.41 in three dimensions. We can now write an expression similar to Eq. (19):

$$\frac{r \nabla P_{\text{cap}}}{P_{\text{cap}}} \approx \frac{\mu q S r^2}{\gamma K k_r} + \frac{(\rho_{\text{w}} - \rho_{\text{nw}})g r^2}{\gamma} = S N_{\text{cap}} / \delta k_r + B \ , \quad (23)$$

and, relating the fractional change in P_{cap} over a length ξ with the change in percolation probability and using $\xi / W \sim (p - p_c)^{-v}$,

$$\xi^{-1-1/v} W^{1/v} \sim \frac{a N_{\text{cap}}}{\delta} \left[\frac{\xi}{W} \right]^{(t-\beta)/v} + aB \ . \quad (24)$$

If we assume that the viscous pressure drop dominates, we ignore the buoyancy term to find

$$\frac{\xi}{W} \sim \left[\frac{W a N_{\text{cap}}}{\delta} \right]^{-v/(1+v+t-\beta)} \ . \quad (25)$$

This expression, without the effect of a finite finger width, was first derived in a different manner by Wilkinson [33]. The exponent in Eq. (25) is approximately -0.25, which means that the correlation length is always fairly small for typical values of the capillary number. Although we cannot test Eq. (25) directly, we expect the variation with finger width to be correctly predicted in this case. We have assumed that for the purposes of calculating the fluid conductance, the pattern looks smooth below a length W—this is reasonable, since, even with small-scale trapping, within a finger, the wetting fluid occupies a significant fraction of the porous medium.

VI. EFFECT OF FLOW IN CREVICES

We will now demonstrate that a small amount of flow in crevices radically alters the displacement pattern. Crevice flow occurs at low flow rates, when the invading fluid is completely wetting (contact angle close to zero), and when the porous medium has connected crevices (heterogeneous soils and consolidated rock). We will assume for this argument that the invading fluid is completely wetting and that flow in crevices is impeded solely by flow rate.

Across a single pore or throat, for the same flow rate, the pressure drop in a crevice is much larger than in a completely filled element. In the numerical model, we have only accounted for pressure drops in the crevices, and ignored them in the filled regions. At very low flow rates, the viscous pressure drops are small in comparison with the capillary pressure. This means that the wetting fluid invades the smallest pores and throats throughout the system. The pressure drop due to flow in crevices is negligible compared with the differences in threshold capillary pressure for pores and throats of different size. At higher flow rates, the pressure drops in both filled regions and in crevices increase. In the numerical model, we continue to assume that the pressure drops in filled portions of the network are small compared to capillary pressure differences, but we do account for the pressure drops in the crevices. As we increase the flow rate, the pressure drop due to crevice flow becomes significant in comparison to the capillary pressure. This means that to fill a throat by snap-off away from the connected front requires an injection pressure that may be sufficient to fill virtually all the pores and throats by connected, frontal advance. In this limit, flow in crevices is suppressed, and we see a connected pattern. Thus, with an increase in flow rate, we see the displacement pattern change from one dominated by snap-off to a connected frontal advance.

The flow in a single crevice that is supplying fluid for throat and pore filling Q is approximately related to the injected flow rate per unit area by $Q = qd^2$, where we have assumed that every throat carries the same average flux. Let us assume that P_{cap} has some representative value γ / r. Moreover, assume that the crevice flow is vertical, where $l = h = dk$, and k is a dimensionless coordinate, denoting distance measured in units of pore lengths. Then if the capillary and Bond numbers are small, Eq. (10) can be written

$$\frac{P_{\text{cap}} - P_0}{P_{\text{cap}}} \approx k(\alpha N_{\text{cap}} + aB) \ . \quad (26)$$

The crevice resistance factor α is typically of order $10^4 - 10^5$, and indicates the large resistance due to flow in crevices compared with flow through fully saturated elements. When αN_{cap} is of order 1, there is a significant fractional change in capillary pressure over just a single pore-throat length and there is essentially no flow in crevices. As the capillary number decreases, more and more filling by snap-off is allowed.

For a large range of pore filling parameters, the displacement pattern with no crevice flow is an almost flat front with some roughness and little or no trapping of the nonwetting phase. This is in accord with experimental evidence [2,16,17]. However, even a small degree of snap-off is sufficient to destroy flat frontal advance, and the cooperative filling mechanisms. For example, Fig. 9 is a sequence of displacement patterns at different capillary numbers. For αN_{cap} of order 1 and larger there is no snap-off, and invasion proceeds by cooperative pore filling with no trapping of nonwetting fluid. Decreasing the flow rate makes the displacement more invasion per-

colationlike. Snap-off a single pore length in advance of the front enables more pores to fill by I_1 and I_2 mechanisms than at higher flow rates. This allows the wetting fluid to fill the smallest pores adjacent to an already filled pore, and lessens the impact of cooperative filling. The transition to flow dominated by snap-off and a percolationlike fluid pattern is not seen until αN_{cap} is of order 10^{-3}, which represents capillary numbers as low as 10^{-8}, typical of many natural fluid displacements. This is consistent with the micromodel experiments of Lenormand and Zarcone [2], who showed that flow dominated by snap-off was only seen for capillary numbers of 10^{-8} and lower.

Correlation length with flow in crevices

We will now use percolation theory to find the correlation length when there is significant flow in crevices. We have already mentioned that, in a single throat, the resistance to flow is much higher through a crevice than if the throat is completely filled. However, if the fluid pattern is percolationlike at breakthrough, the filled regions have a very tenuous structure, and it is possible that across the whole system the pressure drop due to flow in crevices is lower than the pressure drop through the tortuous pathway of filled pores and throats. If this is the case, the pressure drop in crevices, given by Eq. (26), governs the fractional change in capillary pressure with distance. Throats will be filled by snap-off in a bond percolationlike process. The average wetting phase saturation where filled throats and pores are first connected will be of order p_c, and not very small, as with invasion percolation. The finger width will be of order 1, since crevice flow will allow throats to be filled everywhere and will destroy cooperative cluster growth processes. Equating the fractional change in capillary pressure over a distance ξ with $p - p_c$, we find

$$\xi \sim (\alpha N_{\text{cap}} + aB)^{-\nu/(1+\nu)} . \tag{27}$$

Equation (27) applies when the pressure drop in crevices [Eq. (26)] is much lower than that in the connected front [Eq. (23)]. This is so when

$$\frac{aN_{\text{cap}}}{\delta} \xi^{(t-\beta)/\nu} + aB \gg \alpha N_{\text{cap}} + aB , \tag{28}$$

and, using Eq. (27) for ξ,

$$(\alpha N_{\text{cap}} + aB)^{-(t-\beta)/(1+\nu)} \gg \frac{\alpha\delta}{a} . \tag{29}$$

The exponent $(t-\beta)/(1+\nu)$ is approximately 0.85. As we mentioned before, $\alpha\delta/a$ will always be much greater than 1—typically in the range 10–100. Thus Eq. (29) only holds for slow flows, when $aB + \alpha N_{\text{cap}}$ is less than approximately 0.01.

In the numerical model, we do not account for the pressure drop in filled regions. This means that the numerical simulations correctly predict the fluid distribution only up to the correlation length given by Eq. (27). On larger scales, the effects of viscous pressure drops in filled regions become significant.

In contrast, Eq. (25) for the correlation length will only be obeyed when the pressure drop in the connected front is lower than that through the crevices, and hence

$$\alpha N_{\text{cap}} + aB \gg \frac{aN_{\text{cap}}}{\delta} \left[\frac{\xi}{W} \right]^{(t-\beta)/\nu} + aB , \tag{30}$$

and thus, assuming that viscous forces dominate over buoyancy,

$$\frac{\alpha\delta}{a} \gg \left[\frac{WaN_{\text{cap}}}{\delta} \right]^{-(t-\beta)/(1+\nu+t-\beta)} . \tag{31}$$

The exponent $(t-\beta)/(1+\nu+t-\beta)$ is approximately 0.46. When the flow is in neither regime, both crevice flow and the pressure drop in the connected front are significant. Remember that W is itself a function of flow rate. If we take $\alpha\delta/a$ to be around 100, Eq. (31) is true for $WaN_{\text{cap}}/\delta > 0.1$, which represents a high flow rate unless W is very large.

From this section we have shown that for the flow rates of greatest interest in this paper—namely when we see the crossover from crevice to connected flow for αN_{cap} in the range 0.01 to 1, neither Eq. (25) nor (27) are likely to be valid. The numerical model will correctly predict the displacement pattern up to the viscous correlation length, when the effect of the pressure drop in completely filled regions first becomes significant. For the range of flow rates we will study, this represents scales of order 10–100 pore lengths. The three-dimensional simulations of crevice flow will be performed on networks of $32 \times 32 \times 32$ pores and in the parameter range studied are expected to represent the flow patterns accurately.

VII. CHANGE IN RESIDUAL SATURATION WITH FLOW RATE

When there is no flow in crevices, the fluid advance is controlled and impeded by the pores. A narrow pore size distribution, where the pores are similar in size to the throats, leads to cooperative growth, and a small residual saturation. As we saw in Fig. 9, a small degree of snap-off just ahead of the front causes the pattern to become invasion percolationlike when αN_{cap} is of order 0.1. When crevice flow is significant, when αN_{cap} is of order 0.001, the displacement is controlled by the throats, which fill first, followed by cascades of pore filling. The residual saturation in this case is likely to be much larger than for very high flow rates, since the throat filling by snap-off will prevent nonwetting fluid from escaping. The exact change in residual saturation cannot be predicted, since it depends on the exact structure of the pore space and the contact angle, but the network model can explore representative features.

This change in residual saturation with flow rate is a phenomenon that is not described by the two processes that have been previously described, namely mobilization of trapped ganglia [28], and the shift in residual saturation due to a change in the distribution of trapped clusters, as predicted by percolation theory [33] [Eq. (22)].

Both these effects are significant when $(a/\delta)N_{cap}$ is of order 1. The competition between connected advance and crevice flow is governed by αN_{cap}. Since α is typically 10–100 times larger than a/δ (the ratio of the parameters represents the relative resistance of crevice flow versus pistonlike advance), this effect is significant at lower capillary numbers.

Percolation theory can predict the change in residual saturation with flow rate when the finger width is of order 1 and there is no flow in crevices—either because the porous medium does not have connected crevices or roughness (such as smooth bead and sand packs, for in-

stance), or if the injected fluid is not completely wetting. In contrast, the competition between snap-off and the pistonlike advance causes a change in residual saturation only in strongly wetting systems, where flow in crevices can occur, and when the residual saturations for connected fluid advance (large αN_{cap}) and disconnected invasion (small αN_{cap}) are appreciably different.

Figure 10 plots the cumulative distribution of trapped clusters for three-dimensional simulations at two different flow rates. This is an extreme example, where the high flow rate limit is virtually flat advance with very little trapping, while at low flow rates snap-off traps more than
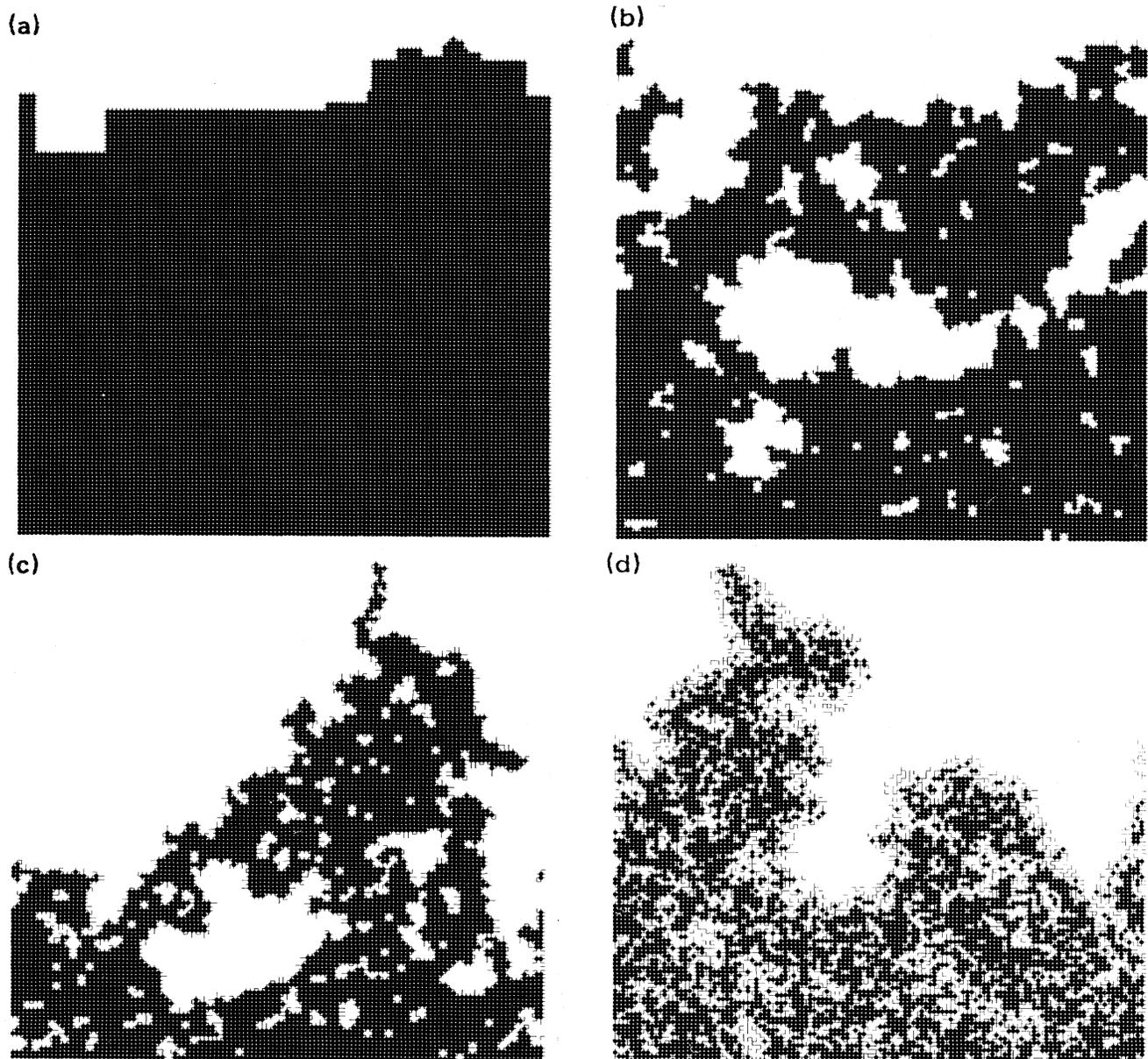
FIG. 9. Two-dimensional simulations of fluid advance, illustrating the effect of the flow rate on the finger width. The simulations are run on a 128×128 grid with different values of αN_{cap}. Both filled pores (circles) and throats (line segments) are shown. (a) $\alpha N_{cap} = 1.7$. (b) $\alpha N_{cap} = 1.7 \times 10^{-1}$. (c) $\alpha N_{cap} = 1.7 \times 10^{-2}$. (d) $\alpha N_{cap} = 1.7 \times 10^{-3}$. (e) $\alpha N_{cap} = 1.7 \times 10^{-4}$.

(e)

FIG. 9. (Continued).

FIG. 11. The fraction of filled pores at breakthrough as a function of flow rate αN_{cap} for three different models. The crosses correspond to the case presented in Fig. 10, where we have a crossover from normal percolation to invasion percolation to almost flat frontal advance with increasing flow rate. The stars represent a case where the high flow rate limit is invasion percolation. The triangles represent a case where the pore and throat sizes are approximately equal, and there is a significant degree of cooperative pore filling at all capillary numbers.

half the pores. There is a sharp transition from percolationlike trapping when $\alpha N_{cap} = 0.05$, to significant suppression of trapping when $\alpha N_{cap} = 0.17$.

Figure 11 shows the fraction of filled pores at breakthrough as a function of flow rate for three different models. The first (shown by crosses) is the case described for Fig. 10, and illustrates the transition from relatively flat frontal advance to invasion percolation to normal percolation as we lower the capillary number. At the lowest flow rates, the fraction of filled pores at breakthrough is close to the percolation threshold, which is approximately 0.31 for a cubic lattice. For αN_{cap} of order 0.001–0.1, the pattern becomes more like invasion percolation over small length scales, and the fraction of filled pores at

breakthrough decreases (for an infinite system, with an infinite viscous correlation length, this fraction would drop to zero). Then sharply, when αN_{cap} is approximately 0.1, the fraction of filled pores rises to a very high value, indicating a flatter fluid advance. The second example, denoted by stars, is similar, except that the high flow rate limit is invasion percolation with a finite finger width. That the fraction of filled pores at breakthrough rises to a fairly high value for $\alpha N_{cap} > 1$ is due to finite size effects. In the third example, the throats are approximately the same size as the pores. We see a crossover from percolation with some cooperative pore filling to an almost flat frontal advance.

Figure 12 shows the finger width as a function of flow rate for the same three examples. The finger width is of order 1 at low flow rates in all three cases. The finger width diverges for cases 1 and 3 for αN_{cap} larger than around 0.1, indicating a locally flat or self-affine growth. Case 2 reaches a finite finger width, indicating locally an invasion percolationlike advance.

Figure 13 shows the residual saturation plotted against flow rate. Since we do not account for ganglion mobilization, or pressure drops in connected regions, we do not see the residual saturation drop to zero for very large capillary number, as observed experimentally [28]. However, for the flow rates representative of natural displacements in porous media—αN_{cap} of order 1 or less—the

FIG. 10. The cumulative trapped cluster distribution plotted as a function of cluster size on doubly logarithmic axes, for different flow rates αN_{cap}.
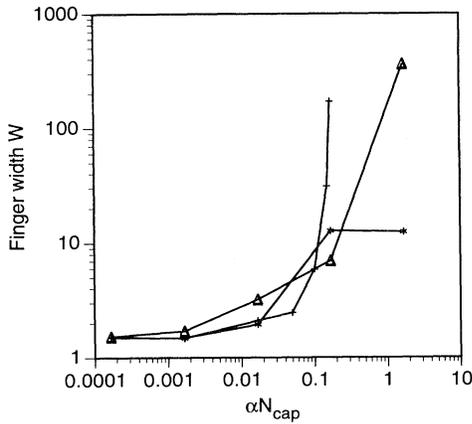
FIG. 12. The finger width as a function of flow rate αN_{cap} for the same three cases as in Fig. 11.
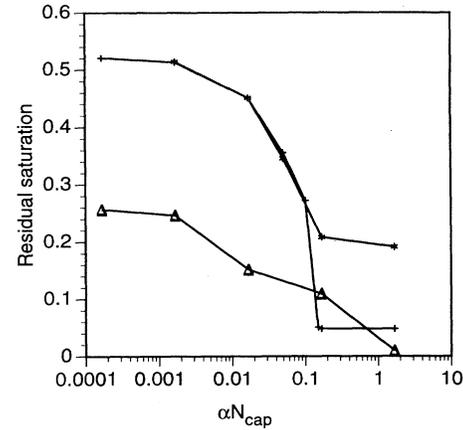
FIG. 13. The residual saturation as a function of flow rate αN_{cap} for the three different systems shown in Figs. 11 and 12.

model does give a realistic indication of the shift on residual saturation with capillary number. The gradual change in residual saturation at very low rates is caused by the transition from a flow regime dominated by snap-off to a connected, invasion percolationlike advance. For the first example, there is a sharp decrease in residual saturation as the finger width diverges at around $\alpha N_{cap} = 0.1$. In the second case, the change in residual saturation with capillary number is the same as in the first case for very low flow rates. Here the displacement is governed by throat filling, and for both examples the distribution of throat sizes is the same. However, the decrease in residual saturation at around $\alpha N_{cap} = 0.1$ is not so dramatic. For the third example, the decrease in residual saturation is more gradual than in the other cases. Notice that for all three examples, the model predicts a noticeable change in residual saturation starting at flow rates around $\alpha N_{cap} = 0.001$ or N_{cap} of order $10^{-8}-10^{-7}$, in the range of many flows in aquifers and reservoirs.

VIII. CONCLUSIONS

We have presented a network model to simulate wetting invasion in a porous medium, including the effects of snap-off, cooperative pore filling, and flow in crevices. We used percolation theory to derive correlation lengths for flow under the perturbative effects of viscous and capillary forces, extending previous work [32,33]. We showed that for displacements with a finger width of order 10 or more, the distribution of trapped nonwetting phase clusters was not in accordance with percolation theory, because of the trapping of clusters that are smaller than the finger width. This means that the derived

correlation lengths could not be used successfully to predict the shift in trapped saturation with flow rate and buoyancy forces.

The competition between crevice flow and pistonlike transport is governed by flow rate. The resistance to flow in crevices is much larger than the resistance through completely filled regions of the pore space, and pore and throat filling well in advance of a connected front only occurs at very low flow rates. The nature of the fluid displacement will change from connected advance (locally resembling invasion percolation, flat frontal advance or self-affine growth on scales below a correlation length) to a disconnected invasion (percolation or nucleated cluster growth) as the flow rate decreases. We showed, using the network model, that an increase in flow rate may dramatically lower the trapped nonwetting phase saturation. The flow rates at which these effects are first significant are when αN_{cap} is of order 0.001. α is a dimensionless crevice resistance factor that depends on the structure of the porous medium, and is typically around 10^4-10^5. This introduces significant changes in local displacement pattern due to flow rate at capillary numbers larger than 10^{-8}, in the range encountered in laboratory experiments and in reservoir and aquifer flows.

[1] M. Sahimi, Rev. Mod. Phys. **65**, 1393 (1993).

[2] R. Lenormand and C. Zarcone, *Society of Petroleum Engineers No. 13264,* in *Proceedings of the 59th Annual Technical Conference of the SPE, Houston* (SPE, Richardson, TX, 1984).

[3] R. Lenormand, C. Zarcone, and A. Sarr, J. Fluid Mech. **135**, 337 (1983).

[4] J. G. Roof, Soc. Pet. Eng. J. **10**, 85 (1970).

[5] N. Martys, M. Cieplak, and M. O. Robbins, Phys. Rev. Lett. **66**, 1058 (1991).

[6] B. Koiller, H. Ji, and M. O. Robbins, Phys. Rev. B **45**, 7762 (1992).

[7] M. J. Blunt, M. J. King, and H. Scher, Phys. Rev. A **46**, 7680 (1992).

[8] R. Lenormand and S. Bories, C. R. Acad. Sci. (Paris) B **291**, 279 (1980).

[9] R. Chandler *et al.*, J. Fluid Mech. **119**, 249 (1982).

[10] D. Wilkinson and J. F. Willemsen, J. Phys. A **16**, 3365 (1983).

[11] R. Lenormand and C. Zarcone, Phys. Rev. Lett. **54**, 2226 (1985).

[12] R. Lenormand and C. Zarcone, in *Kinetics of Aggregation and Gelation,* edited by F. Family and D. P. Landau (Elsevier, Amsterdam, 1984).

[13] H. Ji and M. O. Robbins, Phys. Rev. B **46**, 14 519 (1992).

[14] M. A. Rubio *et al.*, Phys. Rev. Lett. **65**, 1339 (1990).

[15] V. K. Horvath, F. Family, and T. Vicsek, Phys. Rev. Lett. **64**, 1388 (1990).

[16] S. He, G. L. M. K. S. Kahanda, and P. Wong, Phys. Rev. Lett. **69**, 3731 (1992).

[17] S. V. Buldyrev *et al.*, Phys. Rev. A **45**, R8313 (1992).

[18] J. Adler and A. Aharony, J. Phys. A **21**, 1387 (1988).

[19] N. Martys, M. O. Robbins, and M. Cieplak, Phys. Rev. B **44**, 12 294 (1991).

[20] M. Cieplak and M. O. Robbins, Phys. Rev. B **41**, 11 508 (1990).

[21] R. Lenormand, E. Touboul, and C. Zarcone, J. Fluid Mech. **189**, 165 (1988).

[22] M. J. Blunt and P. R. King, Phys. Rev. A **37**, 3935 (1988).

[23] M. J. Blunt and P. R. King, Transp. Porous Media **6**, 407 (1991).

[24] J. Billiotte, H. D. Moegen, and P.-E. Oren, SPE Adv. Tech. Ser. **1**, 133 (1993).

[25] P.-E. Oren, J. Billiotte, and W. V. Pinczewski, in *Society of Petroleum Engineers No. 27814,* in *Proceedings of the 9th SPE/DOE Symposim on Improved Oil Recovery, Tulsa* (SPE, Richardson, TX, 1994).

[26] F. A. L. Dullien, *Porous Media, Fluid Transport and Pore Structure,* 2nd ed. (Academic, San Diego, 1992).

[27] R. Lenormand and C. Zarcone, SPE Form. Eval. **3**, 271 (1988).

[28] N. R. Morrow, I. Chatzis, and J. J. Taber, SPE Reservoir Eng. **3**, 927 (1988).

[29] I. Chatzis and N. R. Morrow, Soc. Pet. Eng. J. **24**, 555 (1984).

[30] A. Abrams, Soc. Pet. Eng. J. **15**, 437 (1975).

[31] R. A. Fulcher, T. Ertekin, and C. D. Stahl, J. Pet. Technol. **25**, 249 (1985).

[32] D. Wilkinson, Phys. Rev. A **30**, 520 (1984).

[33] D. Wilkinson, Phys. Rev. A **34**, 1380 (1986).

[34] D. Zhou and F. M. Orr, In Situ **19**, 249 (1995).

[35] T. C. Ransohoff and C. J. Radke, J. Colloid Interf. Sci. **121**, 392 (1988).

[36] S. Bryant, P. R. King, and D. W. Mellor, Transp. Porous Media **11**, 53 (1993).

[37] S. Bryant and M. J. Blunt, Phys. Rev. A **46**, 2004 (1992).

[38] D. Stauffer and A. Aharony, *Introduction to Percolation Theory,* 2nd ed. (Taylor and Francis, London, 1992).